Batteries

International Edition: DOI: 10.1002/anie.201905794
German Edition: DOI: 10.1002/ange.201905794

Suppressed Mobility of Negative Charges in Polymer Electrolytes with an Ether-Functionalized Anion

Heng Zhang, Fangfang Chen, Oier Lakuntza, Uxue Oteo, Lixin Qiao, Maria Martinez-Ibañez, Haijin Zhu, Javier Carrasco,* Maria Forsyth, and Michel Armand**

Abstract: *Suppressing the mobility of anionic species in polymer electrolytes (PEs) is essential for mitigating the concentration gradient and internal cell polarization, and thereby improving the stability and cycle life of rechargeable alkali metal batteries. Now, an ether-functionalized anion (EFA) is used as a counter-charge in a lithium salt. As the salt component in PEs, it achieves low anionic diffusivity but sufficient Li-ion conductivity. The ethylene oxide unit in EFA endows nanosized self-agglomeration of anions and trapping interactions between the anions and its structurally homologous matrix, poly(ethylene oxide), thus suppressing the mobility of negative charges. In contrast to previous strategies of using anion traps or tethering anions to a polymer/inorganic backbone, this work offers a facile and elegant methodology on accessing selective and efficient Li-ion transport in PEs and related electrolyte materials (for example, composites and hybrid electrolytes).*

The development of safe and high-energy-density batteries is of peculiar importance for approaching a fossil fuel-free and electrified society.[1] The rocking-chair type Li-ion batteries (LIBs), first commercialized by Sony in 1991, have become the most prevalent power sources for portable electronics and electric vehicles (EVs).[2] However, the inherent instability and flammability of carbonate-based liquid electrolytes used in current LIBs not only cause severe safety concerns under abuse conditions but also hamper the integration of the lithium metal (Li^0) anode, which has a circa 10 times higher capacity than the conventional graphite anode and could help boost the energy density of the state-of-art cell technologies.[3]

Owing to their superior flexibility, processability, and immense possibilities in structural design, polymer electrolytes (PEs) are considered to be one of the most promising choices to circumvent the above-mentioned issues encountered in liquid electrolytes.[4] The technological feasibility of PEs as electrolytes for solid-state lithium metal batteries (SSLMBs) has been demonstrated by the expanding implementation of Bluecar and Bluebus powered by a 30 kWh Li° | PE | $LiFePO_4$ (LFP) battery in several cities/countries worldwide (for example, Lyon, Bordeaux, Singapore, and Indianapolis).[5] However, such PE-based SSLMBs are only on a par with conventional LIBs in terms of energy density and rate-capability owing to relatively low areal loadings ($mAh\,cm^{-2}$) of cathode material. In effect, the predominant transport of negative charges (that is, low Li^+ transference number, T_{Li^+}, ca. 0.2) in PEs results in dendritic Li° and poor utilization of active materials in thick electrodes.[3a,c,4c,6]

As summarized in Figure 1, currently, three specific methods have been employed for suppressing the anion mobility, including 1) the addition of anion trap for capturing anions by classic Lewis acid–base interactions (Figure 1 b), for example, boron-based Lewis acid,[7] calix[4]arene,[8] calix[*n*]pyrroles;[9] 2) covalently linking the anions to organic

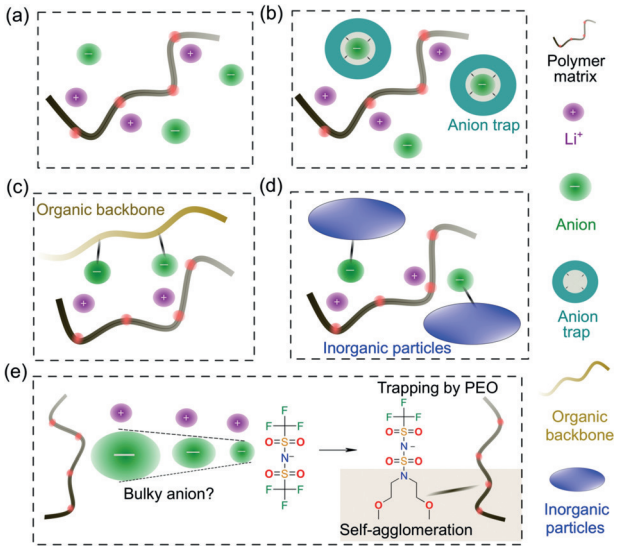

Figure 1. Strategies for suppressing the mobility of anions in PEs: a) traditional PEs; b) adding an anion trap; c) tethering an anion to organic backbone; d) grafting an anion to inorganic particles; and e) our proposed ether-functionalized anion.

[*] Dr. H. Zhang, Dr. O. Lakuntza, U. Oteo, L. Qiao, Dr. M. Martinez-Ibañez, Dr. J. Carrasco, Prof. M. Armand
CIC Energigune, Parque Tecnológico de Álava
Albert Einstein 48, 01510 Miñano, Álava (Spain)
E-mail: hzhang@cicenergigune.com
jcarrasco@cicenergigune.com
marmand@cicenergigune.com
Dr. F. Chen, Dr. H. Zhu, Prof. M. Forsyth
ARC Centre of Excellence for Electromaterials Science (ACES), Institute for Frontier Materials (IFM), Deakin University
Burwood, Victoria 3125 (Australia)
Supporting information and the ORCID identification number(s) for the author(s) of this article can be found under: https://doi.org/10.1002/anie.201905794.

backbones (Figure 1c), for example, polystyrene,[10] polyacrylate,[11] and covalent organic frameworks;[12] and 3) attaching the anions to inorganic particles (Figure 1d), for example, nanosized SiO_2 or Al_2O_3 particles.[13] In the first method, low anion mobility is generally achieved at high expense of total and Li-ion ionic conductivities owing to decreased segmental mobility of the organic backbone upon the addition of rigid anion traps. The latter two methods involve chemically arduous modifications of polymers or inorganic particles for tethering the anions.

The structural modification of anions has long been considered as an efficient and versatile tool for regulating the physicochemical and electrochemical properties of PEs. Yet, Gorecki et al.[14] showed that the introduction of bulkier perfluorinated alkyl chains (up to C_4F_9) in homologues of the widely used bis(trifluoromethanesulfonyl)imide anion ($[N(SO_2CF_3)]_2^-$, TFSI) did not result in any improvement in the selectivity of Li^+ transport (that is, comparable $T_{Li}{}^+$ of ca. 0.2) but a significant drop in both anion and Li^+ mobilities was seen. Herein, we report an ether-functionalized anion (EFA), which contains partial TFSI structure and ethylene oxide (EO) units, respectively (Figure 1e), aiming at suppressing the mobility of negative charges in PEs. Our central hypotheses are 1) the negative charge delocalized by one nitrogen and four oxygen atoms in the presence of electron-withdrawing $-CF_3$ group in sulfonimide center endows a weak coordination nature to EFA, which retains the facile dissociation from Li^+; 2) the inherent structural flexibility of sulfonimide results in a superior plasticizing effect in PEO-based electrolyte, which ensures the high segmental mobility of EO units in polymer backbone upon the addition of lithium salt; and 3) the presence of EO unit in EFA offers potential miscibility between salt anion and its homologous PEO, which may partially link the anion motion to the structural dynamic of polymer matrix, thereby leading to an enhanced selectivity in Li^+ transport as well as a decreased anion mobility.

To examine the electronic structure of the proposed EFA and confirm the plausibility of our central hypotheses, we first performed a series of density functional theory (DFT) calculations. The corresponding optimized geometries are summarized in the Supporting Information, Figure S1 and Table S1. The dissociation energy, ΔE_d, of a LiEFA ion pair at its optimized ground-state geometry, is 675 kJ mol^{-1} (see LiEFA (2#) in Figure 2). This value is significantly larger than the ΔE_d of LiTFSI, 590 kJ mol^{-1}, a direct consequence of the strong affinity of Li ions for ether groups in EFA. In particular, while in LiTFSI the Li ion is bidentately coordinated to one O atom from each sulfonyl group (O_{SG}), our DFT calculations reveal that LiEFA prefers to sacrifice one of these $Li-O_{SG}$ bonds and form instead an O-tridentate structure with the two O atoms of each ether groups (O_{EG}) and one remaining O_{SG}. Interestingly, from an electronic structure viewpoint, the substitution in LiTFSI of one $-CF_3$ group, with its strong electron withdrawn ability,[15] by $-N[(CH_2CH_2O)CH_3]_2$ has only a moderate impact on ΔE_d; in particular, the ΔE_d of a metastable LiEFA ion pair with only bidentate coordination to two O_{SG} [LiEFA (1#) in Figure 2], is 617 kJ mol^{-1}, that is, 27 kJ mol^{-1} higher than that of LiTFSI. Overall, EFA is able to offer Li ions four effective O coordination sites (two from the sulfonyl groups and two from the ether groups) and the structural flexibility of the EO-type side chains facilitates the formation of strongly bonded tridentate structures. Yet, a key observation in this analysis is that the complete saturation of the four O sites (that is, formation of tetradentate structures) is not possible because of structural constrains (geometry optimization attempts to obtain tetradentate structures always resulted in bidentate and tridentate geometries). This suggests that at least one of the four O sites present in each EFA could effectively participate in intermolecular EFA-PEO interactions and, therefore, hindering EFA mobility.

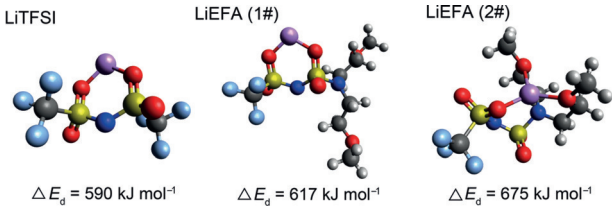

Figure 2. Optimized geometries of LiTFSI and LiEFA. O red, S yellow, F light blue, N dark blue, C gray, H light gray, Li purple.

Inspired by the above theoretical insights, EFA-based salt LiEFA was facilely synthesized via commercially available intermediates (see the Supporting Information, Scheme S1 for the synthetic route and Figure S2 for NMR characterization). Self-standing membranes are easily prepared for the electrolytes with moderate salt content (EO/Li > 12; see the Supporting Information, Figure S3 for physical appearances). As seen in Figure 3a, LiEFA/PEO decomposes thermally at a slightly lower temperature than LiTFSI/PEO due to the thermal lability of $-N(CH_2CH_2OCH_3)_2$ group vs. $-CF_3$ moiety, which is supported by the lower decomposition temperature (T_d) of the neat salt (that is, $T_d = 308\,°C$ (LiEFA) vs. $T_d = 367\,°C$ (LiTFSI), Figure S4). However, the thermal stability of LiEFA/PEO is well acceptable for the scalable processing (for example, extrusion at temperatures $< 200\,°C$) and operation of polymer-based lithium batteries ($< 100\,°C$).

The semi-crystalline nature of LiEFA/PEO and LiTFSI/PEO is clearly depicted by the XRD patterns (Supporting Information, Figure S5) and DSC traces (Figure 3b; Supporting Information, Figure S6), where characteristic diffraction peaks at about 19°, 23° and melting transitions at about 60 °C assigned to the crystalline PEO phase, together with glass transitions between −46 °C and −32 °C associated with the amorphous PEO phase are observed. Interestingly, LiEFA/PEO (20) shows a glass transition (T_g) at −35 °C and a crystallinity (χ_c) of 49 %, both of which are comparable to the respective values of LiTFSI/PEO (20) (that is, $T_g = -36\,°C$ and $\chi_c = 52\,\%$), indicating a similar segmental mobility of PEO in both electrolytes. With a higher salt concentration, the difference between LiEFA and LiTFSI on plasticizing the PEO matrix appears to be more distinctive, that is, LiTFSI/PEO at EO/Li = 8 becomes fully amorphous while LiEFA/PEO at the same concentration shows a high crystallinity of 48 % (Supporting Information, Table S2). This could be ascribed to stronger interactions between EFA and PEO via

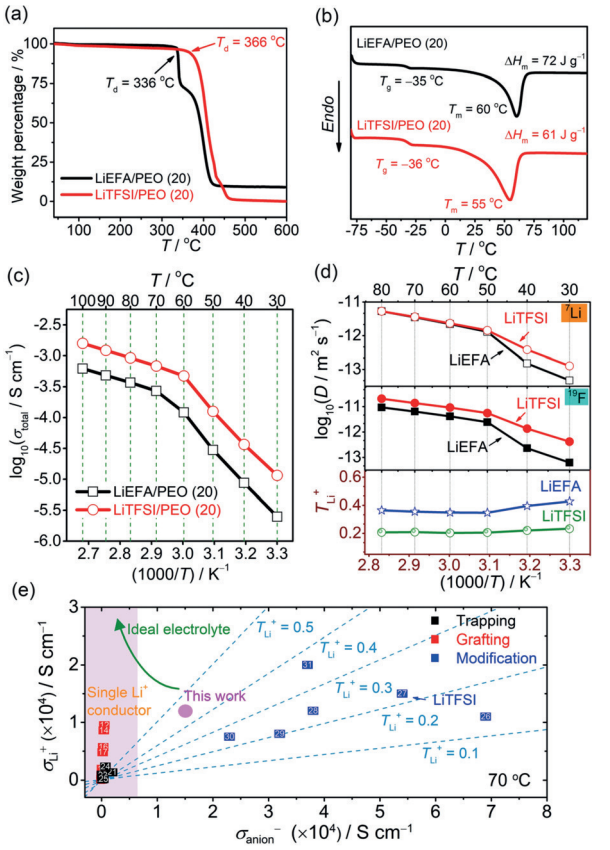

Figure 3. Physicochemical properties of LiEFA- and LiTFSI-based electrolytes. a) Thermogravimetric analysis (TGA); b) differential scanning calorimetry (DSC) traces; c) Arrhenius plot of total ionic conductivity (σ_{total}); d) temperature dependence of diffusion coefficient and T_{Li}^+ measured by PFG NMR; e) Li-ion (σ_{Li}^+) and anionic (σ_{anion}^-) conductivity of the state-of-art PE electrolytes. An enlargement of the left lower corner is given in the Supporting Information, Figure S9. The numbers in squares in (e) correspond to the entries listed in the Supporting Information, Table S4, and color code corresponds to the method used for suppressing anion motion.

EO units, inducing further rigidity on segmental motion of PEO-based electrolyte.

Figure 3c compares the total ionic conductivity (σ_{total}) of LiEFA/PEO and LiTFSI/PEO at the same EO/Li ratio of 20 (see the Supporting Information, Figure S7 for other concentrations). In general, the LiEFA-based electrolytes exhibit their highest conductivity at the salt content of EO/Li = 20 due to the trade-off between the number of charge carriers and their diffusivity, as observed by Prud'homme et al. for LiTFSI/PEO.[16] At the salt content of EO/Li = 20, the values of σ_{total} for LiEFA/PEO drop three times compared to LiTFSI/PEO, as expected by the larger anion size of EFA. However, pulsed-field gradient nuclear magnetic resonance (PFG NMR) measurements show that the Li^+ diffusivity in LiEFA/PEO is almost superimposable to that of LiTFSI/PEO, while the diffusivity of the anion decreases dramatically in LiEFA/PEO (Figure 3d), implying that the lower σ_{total} in LiEFA/PEO is related to the suppressed mobility of EFA. In consequence, the Li-ion transference number (T_{Li}^+) of LiEFA/PEO is significantly higher than that of LiTFSI/PEO, as further testified by the electrochemical polarization tests where a higher value of T_{Li}^+ is obtained for LiEFA/PEO ($T_{Li}^+ = 0.43$ (LiEFA/PEO; Supporting Information, Table S3 and Figure S8) vs. 0.22 (LiTFSI/PEO)[17]).

As shown in Figure 3e, most of the strategies towards approaching unity Li-ion transport lead to a dramatic drop in σ_{total} and Li-ion conductivity, for example, tethering TFSI-like (that is, $CF_3SO_2N^{(-)}SO_2-$) anions to a polystyrene backbone yield the PE with ionic conductivity as low as 1×10^{-5} S cm^{-1} though the selectivity of Li-ion transport was improved,[10a] and further improvement in conductivity requires super delocalized anionic structures which are only accessible via laborious synthetic routes.[10d] In sharp contrast, LiEFA/PEO shows the untouched high mobility of Li^+ and greatly suppressed anion mobility (see the Supporting Information, Figure S10 for clear comparison with LiTFSI-based electrolytes), which surpasses other kinds of PEs.

To unravel the unique role of structural design of anions on ionic conductivity and shed light on the transport mechanism of ions in PEO-based electrolytes, both LiEFA/PEO and LiTFSI/PEO systems at the salt content of EO/Li = 20 were studied by molecular dynamic (MD) simulations (see the Supporting Information, Table S5, Figures S11, S12 for detailed MD information). Figure 4a displays the radial distribution function (RDF) and distance-dependent coordination number (CN) for analyzing the Li^+ coordination environment, especially with the oxygen atom from both PEO and anions. For both LiEFA/PEO and LiTFSI/PEO, the Li-O (PEO) RDF presents a sharp first peak at a position significantly lower (that is, 1.7–3.3 Å) than that of Li–O (EFA or TFSI) RDF (5.1–9.9 Å), suggesting that Li^+ cations are fully solvated and predominately wrapped by the PEO backbone and neither the oxygen of SO_2 in sulfonimide center nor the EO unit present in EFA contributes to the complexation of Li^+. The preferred interaction between Li^+ and PEO was confirmed from MD simulations by Borodin et al. in several LiX/PEO systems (X = I, PF_6, BF_4, TFSI).[18] A quantitative characterization of ion motion via the mean square displacement (MSD) is shown in Figure 4b. The MSD of anions (F atom) decreases dramatically with the replacement of $-CF_3$ with $-N[(CH_2CH_2O)CH_3]_2$, strongly implying lower diffusivity of EFA compared to that of TFSI, whereas such a structural change in anion has a small impact on dynamics of lithium ions. This is in agreement with our PFGNMR results (Figure 3d) and further testifies to the suppressed mobility of negative charges in EFA-based electrolytes. Figure 4c,d depicts the snapshot from MD simulations for revealing nearest coordination environment of lithium ions in both electrolytes. The coordination structures within 5 Å (around the first valley of the Li–O RDF) of lithium ions are highlighted by molecular surface maps which are completely derived from PEO structures. Both EFA (yellow ball and stick) and TFSI (orange ball and stick) are all found outside this coordination range. One may note that EFA is partially self-agglomerated and trapped by the PEO backbone (Supporting Information, Figure S11a,b), and the stable EFA-EFA and EFA-PEO structures are also confirmed by DFT calculations (Supporting Information, Figure S11c,d); while TFSI is homogenously distributed outside

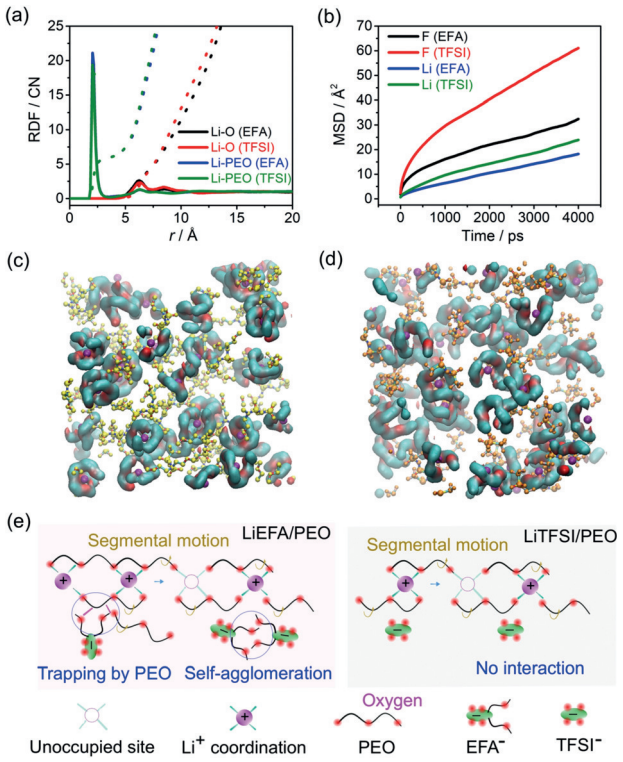

Figure 4. Molecular dynamics simulations and ion transport mechanisms of LiEFA/PEO and LiTFSI/PEO. a) Radial distribution function (RDF, solid line) calculated between Li and O from either PEO or anion (EFA or TFSI) and their coordination number (CN, dotted line); b) mean-square displacement (MSD) of Li^+ and F atoms in anions; c),d) snapshots of the coordination environment of the lithium ions within 5 Å (molecular surface map) as well as all anions (ball and stick) from MD simulations of c) LiEFA/PEO and d) LiTFSI/PEO systems at 353 K; EFA and TFSI are shown in the ball and stick model (O red, S yellow, F pink, N dark blue, C aqua, H white), PEO is presented by the surface map. e) Illustration of the ionic transport mechanism.

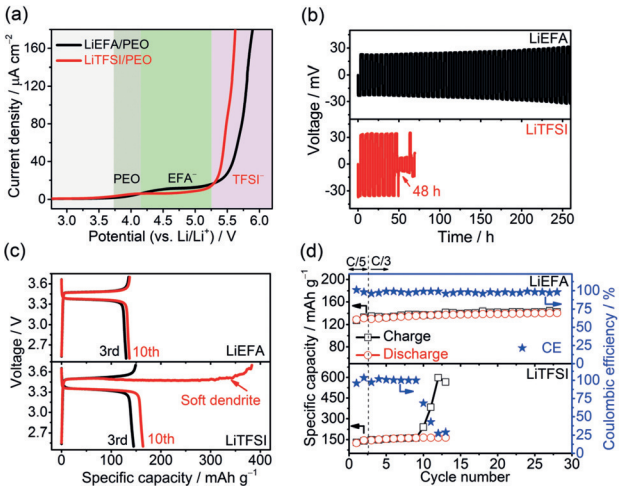

Figure 5. Electrochemical properties of LiEFA/PEO and LiTFSI/PEO at 70 °C. a) Linear sweeping voltammetry profiles measured on stainless steel electrode at a scan rate of 1 $mV s^{-1}$; b) galvanostatic cycling of Li^0 symmetric cells at 0.1 $mA cm^{-2}$ (half cycle time 3 h), a zoomed-in plot is available in the Supporting Information, Figure S14; c) charge/discharge profiles of Li^0 || $LiFePO_4$ cells at a rate of C/3; d) specific capacity and Coulombic efficiency vs. cycle number of Li^0 || $LiFePO_4$ cells (two formation cycles at C/5 and then constant cycles at C/3).

the shell of Li-PEO complex. The RDF and CN of H–O clearly shows that EFA interacts with PEO chain via hydrogen bonding interaction formed by CH_2 units in PEO and ether (O_{EG}) or sulfonyl group (O_{SG}) in EFA (Supporting Information, Figure S11e). As illustrated in Figure 4e, EFA ions form aggregates via the affinity of EO units, meanwhile, such affinity allows the interactions between the EO unit from EFA and PEO, thereby slowing down the diffusion and mobility of negative charges.

To demonstrate the feasibility of LiEFA as conducting salt for SSLMBs, the electrochemical properties of LiEFA/PEO (20) are further investigated in terms of anodic stability, compatibility with Li^0 electrode, and cycling performance of Li^0 || $LiFePO_4$ cells. As shown in Figure 5a, both LiEFA/PEO and LiTFSI/PEO show oxidation currents at ca. 4.0 V vs. Li/Li^+, owing to the decomposition of PEO.[19] The slightly higher intensity of anodic current in the range of 4–5 V implies a lower anodic stability of LiEFA vs. LiTFSI, which is confirmed by the lower oxidation potential of LiEFA/propylene carbonate solution (Supporting Information, Figure S13). This could be ascribed to the stronger electron-withdrawing ability and electrochemical inertness of $-CF_3$ vs. $-N[(CH_2CH_2O)CH_3]_2$. However, LiEFA is electrochemically stable enough for circa 4 V class batteries (for example, Li-S, Li-V_2O_5, Li-$LiFePO_4$).[17]

Figure 5b depicts the galvanostatic cycling of Li^0 symmetric cells using both electrolytes. The voltage profile of the LiEFA-based cell remains stable for more than 250 h, while that of the LiTFSI-based one suffers from short-circuit after only 48 h (see the Supporting Information, Figure S14 for the zoomed-in plot). This suggests a remarkably enhanced stability of Li^0 electrode in the former electrolyte. Furthermore, the electrochemical performances of the Li^0 || $LiFePO_4$ cells using LiEFA/PEO and LiTFSI/PEO are evaluated. As seen in Figure 5c,d, the LiEFA-based cell shows stable charge/discharge profiles with high Coulombic efficiencies for more than 25 cycles (Figure 5d); however, the LiTFSI-based one shows prolonged charging process beyond the 10th cycles (Figure 5c), owing to the formation of soft dendrites on Li^0 anode.[19] Such superior electrochemical performance of the LiEFA-based cell could be ascribed to 1) the suppressed mobility of negative charges upon the functionalization of the sulfonimide anion with an ether group, which decreases the concentration polarization of the cell, thus mitigating the formation of dendritic Li^0; and 2) the formation of stable solid electrolyte interphase (SEI) layer on Li^0 anode, which enables efficient Li^+ transport through electrolyte/electrode interphase and thereby minimizing the side reaction between electrolyte and Li^0 anode. Further morphological and compositional studies on the Li^0 anode cycled in the LiEFA-based electrolyte are currently undergoing for gaining an in-depth understanding of anion chemistry on Li^0 anode.

In summary, we have designed and prepared easily an ether-functionalized anion (EFA) for attaining high Li-ion conductivity with significantly suppressed anion mobility in

PEs. DFT calculations on the electronic structure of pristine LiEFA suggest slightly increased dissociation energy due to the additional coordination of Li^+ via EO unit in EFA. Apart from its processability and good thermal stability, LiEFA/PEO possesses fast and selective Li-ion transport, achieving a high Li-ion conductivity of $1.2\times10^{-4}\,S\,cm^{-1}$ with an extremely low anionic conductivity (6 times lower than that of the LiTFSI-based one at 70 °C). As elucidated by MD simulations, such outstanding transport behavior is attributed to the affinity of EO units in EFA, which promotes the self-agglomeration of anions and interactions with PEO, impeding the diffusion and motion of negative charges. These advantageous properties of the LiEFA-based electrolytes enable the stable cycling of Li^0 electrode and an improved performance of Li^0 || $LiFePO_4$ cell. This work provides an efficient and scalable strategy for accessing low anion mobility, highly Li-ion conductive PEs, which are urgently needed for building high-performance solid-state lithium batteries and other rechargeable batteries such as sodium batteries.

Acknowledgements

This work was supported by the Ministerio de Economía y Competitividad (MINECO) of the Spanish Government through Proyectos I + D Retos program (ENE2015-64907C2-1-R and ENE2016-81020-R grants) and the European Union's Horizon 2020 research and innovation programme under grant agreement No 769929. We also acknowledge funding by the Basque Government through the GVEL-KARTEK-2016 program. H.Z. thanks the Basque Government for the Berrikertu program (1-AFW-2017-2) and L.Q. gratefully acknowledges the financial support from Chinese Scholarship Council (no.201808370162). F.C. acknowledges the assistance of resources and services from the National Computational Infrastructure (NCI), supported by Australian Government. We are also grateful for computer resources to the i2BASQUE academic network and SGI/IZOSGIker UPV/EHU (Arina cluster). Deakin University's Advanced Characterization Facility is acknowledged for use of the NMR instruments. We thank Neware (Shenzhen, China) for offering the battery cycler.

Conflict of interest

The authors declare no conflict of interest.

Keywords: batteries · electrolytes · ether-functionalized anions · negative charge mobility

How to cite: *Angew. Chem. Int. Ed.* **2019**, *58*, 12070–12075
Angew. Chem. **2019**, *131*, 12198–12203

[1] a) M. Armand, J.-M. Tarascon, *Nature* **2001**, *414*, 359 – 367; b) M. Armand, J.-M. Tarascon, *Nature* **2008**, *451*, 652 – 657.

[2] a) J. B. Goodenough, K. S. Park, *J. Am. Chem. Soc.* **2013**, *135*, 1167 – 1176; b) A. Yoshino, *Angew. Chem. Int. Ed.* **2012**, *51*, 5798 – 5800; *Angew. Chem.* **2012**, *124*, 5898 – 5900; c) J. B. Goodenough, *Nat. Electron.* **2018**, *1*, 204 – 204.

[3] a) W. Xu, J. Wang, F. Ding, X. Chen, E. Nasybulin, Y. Zhang, J.-G. Zhang, *Energy Environ. Sci.* **2014**, *7*, 513 – 537; b) J. Janek, W. G. Zeier, *Nat. Energy* **2016**, *1*, 16141; c) X.-B. Cheng, R. Zhang, C.-Z. Zhao, Q. Zhang, *Chem. Rev.* **2017**, *117*, 10403 – 10473; d) S. Xia, X. Wu, Z. Zhang, Y. Cui, W. Liu, *Chem* **2019**, *5*, 753 – 785.

[4] a) V. Di Noto, S. Lavina, G. A. Giffin, E. Negro, B. Scrosati, *Electrochim. Acta* **2011**, *57*, 4 – 13; b) D. T. Hallinan, N. P. Balsara, *Annu. Rev. Mater. Res.* **2013**, *43*, 503 – 525; c) H. Zhang, C. Li, M. Piszcz, E. Coya, T. Rojo, L. M. Rodriguez-Martinez, M. Armand, Z. Zhou, *Chem. Soc. Rev.* **2017**, *46*, 797 – 815.

[5] http://www.bollore.com/en-us/activities/electricity-storage-and-solutions/blue-applications.

[6] a) J. N. Chazalviel, *Phys. Rev. A* **1990**, *42*, 7355 – 7367; b) M. Doyle, T. F. Fuller, J. Newman, *Electrochim. Acta* **1994**, *39*, 2073 – 2081.

[7] a) M. A. Mehta, T. Fujinami, *Chem. Lett.* **1997**, *26*, 915 – 916; b) R. Kurono, M. A. Mehta, T. Inoue, T. Fujinami, *Electrochim. Acta* **2001**, *47*, 483 – 487; c) Y. Yang, T. Inoue, T. Fujinami, M. A. Mehta, *Solid State Ionics* **2001**, *140*, 353 – 359.

[8] a) A. Blazejczyk, W. Wieczorek, R. Kovarsky, D. Golodnitsky, E. Peled, L. G. Scanlon, G. B. Appetecchi, B. Scrosati, *J. Electrochem. Soc.* **2004**, *151*, A1762 – A1766; b) A. Blazejczyk, M. Szczupak, W. Wieczorek, P. Cmoch, G. B. Appetecchi, B. Scrosati, R. Kovarsky, D. Golodnitsky, E. Peled, *Chem. Mater.* **2005**, *17*, 1535 – 1547.

[9] a) M. Kalita, M. Bukat, M. Ciosek, M. Siekierski, S. H. Chung, T. Rodríguez, S. G. Greenbaum, R. Kovarsky, D. Golodnitsky, E. Peled, D. Zane, B. Scrosati, W. Wieczorek, *Electrochim. Acta* **2005**, *50*, 3942 – 3948; b) A. Plewa, F. Chyliński, M. Kalita, M. Bukat, P. Parzuchowski, R. Borkowska, M. Siekierski, G. Z. Żukowska, W. Wieczorek, *J. Power Sources* **2006**, *159*, 431 – 437.

[10] a) R. Meziane, J.-P. Bonnet, M. Courty, K. Djellab, M. Armand, *Electrochim. Acta* **2011**, *57*, 14 – 19; b) M. S. Bouchet, R. Meziane, A. Aboulaich, L. Lienafa, J. P. Bonnet, T. N. T. Phan, D. Bertin, D. Gigmes, D. Devaux, R. Denoyel, M. Armand, *Nat. Mater.* **2013**, *12*, 452 – 457; c) S. Feng, D. Shi, F. Liu, L. Zheng, J. Nie, W. Feng, X. Huang, M. Armand, Z. Zhou, *Electrochim. Acta* **2013**, *93*, 254 – 263; d) Q. Ma, H. Zhang, C. Zhou, L. Zheng, P. Cheng, J. Nie, W. Feng, Y.-S. Hu, H. Li, X. Huang, L. Chen, M. Armand, Z. Zhou, *Angew. Chem. Int. Ed.* **2016**, *55*, 2521 – 2525; *Angew. Chem.* **2016**, *128*, 2567 – 2571.

[11] a) L. Porcarelli, A. S. Shaplov, F. Bella, J. R. Nair, D. Mecerreyes, C. Gerbaldi, *ACS Energy Lett.* **2016**, *1*, 678 – 682; b) M. Piszcz, O. Garcia-Calvo, U. Oteo, J. M. Lopez del Amo, C. Li, L. M. Rodriguez-Martinez, H. B. Youcef, N. Lago, J. Thielen, M. Armand, *Electrochim. Acta* **2017**, *255*, 48 – 54.

[12] a) Y. Hu, N. Dunlap, S. Wan, S. Lu, S. Huang, I. Sellinger, M. Ortiz, Y. Jin, S. H. Lee, W. Zhang, *J. Am. Chem. Soc.* **2019**, *141*, 5880 – 5885; b) K. Jeong, S. Park, G. Y. Jung, S. H. Kim, Y.-H. Lee, S. K. Kwak, S.-Y. Lee, *J. Am. Chem. Soc.* **2019**, *141*, 7518 – 7525.

[13] a) N. Lago, O. Garcia-Calvo, J. M. Lopez del Amo, T. Rojo, M. Armand, *ChemSusChem* **2015**, *8*, 3039 – 3043; b) H. Zhao, F. Asfour, Y. Fu, Z. Jia, W. Yuan, Y. Bai, M. Ling, H. Hu, G. Baker, G. Liu, *ACS Appl. Mater. Interfaces* **2015**, *7*, 19494 – 19499; c) H. Zhao, Z. Jia, W. Yuan, H. Hu, Y. Fu, G. L. Baker, G. Liu, *ACS Appl. Mater. Interfaces* **2015**, *7*, 19335 – 19341.

[14] W. Gorecki, M. C. C. Roux, M. Armand, E. Belorizky, *ChemPhysChem* **2002**, *3*, 620 – 625.

[15] H. Zhang, O. Arcelus, J. Carrasco, *Electrochim. Acta* **2018**, *280*, 290 – 299.

[16] M. P. S. Lascaud, A. Vallke, S. Besner, J. Prud'homme, M. Armand, *Macromolecules* **1994**, *27*, 7469 – 7477.

[17] H. Zhang, U. Oteo, H. Zhu, X. Judez, M. Martinez-Ibañez, I. Aldalur, E. Sanchez-Diez, C. Li, J. Carrasco, M. Forsyth, M.

Armand, *Angew. Chem. Int. Ed.* **2019**, *58*, 7829 – 7834; *Angew. Chem.* **2019**, *131*, 7911 – 7916.
[18] a) O. Borodin, G. D. Smith, *Macromolecules* **1998**, *31*, 8396 – 8406; b) O. Borodin, G. D. Smith, R. L. Jaffe, *J. Comput. Chem.* **2001**, *22*, 641 – 654; c) O. Borodin, G. D. Smith, R. Douglas, *J. Phys. Chem. B* **2003**, *107*, 6824 – 6837; d) O. Borodin, G. D. Smith, *Macromolecules* **2006**, *39*, 1620 – 1629; e) D. Diddens, A. Heuer, O. Borodin, *Macromolecules* **2010**, *43*, 2028 – 2036.
[19] a) I. Aldalur, M. Martinez-Ibañez, M. Piszcz, L. M. Rodriguez-Martinez, H. Zhang, M. Armand, *J. Power Sources* **2018**, *383*, 144 – 149; b) I. Aldalur, M. Martinez-Ibañez, A. Krztoń-Maziopa, M. Piszcz, M. Armand, H. Zhang, *J. Power Sources* **2019**, *423*, 218 – 226.

Manuscript received: May 10, 2019
Revised manuscript received: June 24, 2019
Accepted manuscript online: July 1, 2019
Version of record online: August 5, 2019

